NeuroImage 188 (2019) 59–69

Contents lists available at ScienceDirect

NeuroImage

journal homepage: www.elsevier.com/locate/neuroimage

Development of population receptive fields in the lateral visual stream improves spatial coding amid stable structural-functional coupling

Jesse Gomez [a,*], Alexis Drain [b], Brianna Jeska [b], Vaidehi S. Natu [b], Michael Barnett [b,c], Kalanit Grill-Spector [b,d]

[a] Neurosciences Program, Stanford University School of Medicine, CA, 94305, USA
[b] Psychology Department, Stanford University, CA, 94305, USA
[c] Psychology Department, University of Pennsylvania, PA, USA
[d] Stanford Neurosciences Institute, Stanford University, CA, 94305, USA

A B S T R A C T

Human visual cortex encompasses more than a dozen visual field maps across three major processing streams. One of these streams is the lateral visual stream, which extends from V1 to lateral-occipital (LO) and temporal-occipital (TO) visual field maps and plays a prominent role in shape as well as motion perception. However, it is unknown if and how population receptive fields (pRFs) in the lateral visual stream develop from childhood to adulthood, and what impact this development may have on spatial coding. Here, we used functional magnetic resonance imaging and pRF modeling in school-age children and adults to investigate the development of the lateral visual stream. Our data reveal four main findings: 1) The topographic organization of eccentricity and polar angle maps of the lateral stream is stable after age five. 2) In both age groups there is a reliable relationship between eccentricity map transitions and cortical folding: the middle occipital gyrus predicts the transition between the peripheral representation of LO and TO maps. 3) pRFs in LO and TO maps undergo differential development from childhood to adulthood, resulting in increasing coverage of the central visual field in LO and of the peripheral visual field in TO. 4) Model-based decoding shows that the consequence of pRF and visual field coverage development is improved spatial decoding from LO and TO distributed responses in adults vs. children. Together, these results explicate both the development and topography of the lateral visual stream. Our data show that the general structural-functional organization is laid out early in development, but fine-scale properties, such as pRF distribution across the visual field and consequently, spatial precision, become fine-tuned across childhood development. These findings advance understanding of the development of the human visual system from childhood to adulthood and provide an essential foundation for understanding developmental deficits.

1. Introduction

Human visual cortex encompasses more than a dozen visual field maps (Wandell and Winawer, 2011; Wang et al., 2015) across three processing streams: ventral, lateral, and dorsal (Battelli et al., 2007; Goodale et al., 1991; Ungerleider and Mishkin, 1982; Weiner and Grill-Spector, 2013). Neurons in these regions have receptive fields that process visual information in specific locations of the visual field, which are organized in a series of topographic maps (Wandell and Winawer, 2011). As neurons with similar receptive fields are clustered, we can measure the population receptive field (pRF) spanned by the collection of neurons in a voxel using fMRI (Dumoulin and Wandell, 2008). Indeed, the characteristics of pRFs and visual field maps in the human brain have been extensively studied in adults (Wandell and Winawer, 2015). However, how pRFs and visual field maps develop during childhood is poorly understood.

Three studies have investigated development of visual field maps in early visual cortex (Conner et al., 2004; Dekker et al., 2017; Gomez et al., 2018). These studies reported adult-like visual field maps in early visual areas V1–V3 in children as young as 5–7 years of age. To date, only one recent study from our lab has examined pRFs in the child's ventral stream. While we found qualitatively similar visual field maps in children and adults, we found quantitative differences between age groups that varied across the ventral visual stream (Gomez et al., 2018). Specifically, while children's pRFs and visual field coverage (VFC) in V1–hV4 were adult-like by age 5, the foveal bias and VFC of face- and word-selective regions increased from childhood to adulthood. However, it is unknown if this pattern of development—namely protracted development of high-level regions and increased foveal coverage – occurs in other processing streams.

We sought to address these important questions by examining the development of visual field maps, pRFs, and VFC in the lateral processing stream (Weiner and Grill-Spector, 2013), which extends from V1 to lateral-occipital (LO (Larsson and Heeger, 2006)) and temporal-occipital (TO (Amano et al., 2009)) visual field maps. The lateral stream is of interest for two reasons. First, its end-stages contain a series of visual field maps

* Corresponding author.
E-mail address: gomezj@stanford.edu (J. Gomez).

https://doi.org/10.1016/j.neuroimage.2018.11.056
Received 2 July 2018; Received in revised form 25 November 2018; Accepted 30 November 2018
Available online 1 December 2018

arranged in two clusters: the LO cluster (LO1/LO2) and the TO cluster (TO1/TO2), which characteristics have been well-studied in adults (Amano et al., 2009; Kay et al., 2013; Larsson and Heeger, 2006; Sayres and Grill-Spector, 2008; Weiner and Grill-Spector, 2011). Importantly, the LO cluster is thought to process object form (Grill-Spector et al., 2001, 1998b; Kourtzi and Kanwisher, 2000; Malach et al., 1995; Mendola et al., 1999; Vinberg and Grill-Spector, 2008), a type of visual processing that is thought to rely on central vision (Strappini et al., 2017). The TO cluster, involved in motion processing, is relatively less centrally biased with large receptive fields extending well into the periphery and ipsilateral visual field (Amano et al., 2009; Huk et al., 2002; Raiguel et al., 1995). This gives us an opportunity to test if there are different patterns of pRF development (central versus more peripheral) within what is classically considered a single visual stream. We thus predict foveal development in LO and more peripherally-biased development in TO. Second, prior studies suggest that higher-level regions in the lateral stream develop earlier than ventral temporal cortex (VTC). Specifically, the hMT + complex (Huk et al., 2002; Tootell et al., 1995a), which overlaps the TO cluster, is thought to be myelinated at birth (Watson et al., 1993). Similarly, object-selective LO (Grill-Spector et al., 1998b; Malach et al., 1995) shows adult-like selectivity to objects (Golarai et al., 2007; Scherf et al., 2007) and faces (Natu et al., 2016) by age 7, even as selectivity to faces and words continue to develop in VTC (Ben-Shachar et al., 2011; Cantlon et al., 2011; Golarai et al., 2007; Scherf et al., 2007). Thus, given the functional contrast between the lateral and ventral streams, the lateral stream presents an opportunity to study if different processing streams implement different forms of pRF development.

Here, we investigated the development of pRFs and visual fields maps in the lateral stream using a pRF mapping experiment in 26 children (ages 5–12), and 26 adults (ages 22–28). We considered the following predictions of competing developmental hypotheses. First, there may be no development of pRFs or visual field maps in higher-level regions of the lateral stream, as functional properties of these regions are reported to be early-developed. Second, in the presence of pRF development, we hypothesize that pRFs of the LO cluster will develop with a bias towards covering the center of the visual field mirroring the use of central vision for object recognition, while pRF development of the TO cluster will be more prominent in the periphery of the visual field, which is over-represented particularly in the TO cluster (Huk et al., 2002).

2. Materials and methods

2.1. Subjects

26 neurologically typical children aged 5–12 years (mean age 8.5 ± 2.2 years, 12 females) and 26 adults ages 22–28 years old (mean age 24 ± 1.6 years, 9 females) participated in these experiments. Data from these subjects were also reported here: (Gomez et al., 2018). Age ranges were chosen in children to (i) maximize a wide dynamic range of functional and structural development reported previously (Cantlon et al., 2011; Golarai et al., 2007; Peelen et al., 2009; Scherf et al., 2007), and (ii) maximize the success of fMRI measurements without having to discard a substantial number of participants due to excessive motion in the scanner, which is a common issue with pediatric neuroimaging (Grill-Spector et al., 2008). Because our goal was to estimate population receptive fields (pRFs) with high precision, and our experiments required maintaining central fixation, we could not make measurements on younger children where acquiring such data is unfeasible. A similar range of ages was chosen in adults when most structural and functional development in visual cortex is thought to be near completion (Golarai et al., 2010; Yeatman et al., 2014). Participants had normal or corrected-to-normal vision and were screened to have no prior or current psychiatric conditions. All procedures were approved to be in accordance with the Institutional Review Board of Stanford University. Prior to the experiment, adult participants and parents provided written informed consent, and children provided written assent.

Each subject participated in several sessions completed over the course of a few months to distribute measurements and avoid fatigue. Each of the following sessions was thus performed on a different day: (i) Participants under the age of 18 completed training in a mock scanner employing live feedback of head motion during the viewing of a 15-min movie. This acclimated the participants to the scanner environment and reduced motion. Participants were advanced to functional and anatomical scanning if they could lie still (less than 2.4 mm of head motion) for the duration of mock scanning. (ii) All participants participated in an MRI session in which we obtained anatomical MRI brain volumes which were used to register data across sessions and obtain cortical surface reconstructions of each brain. (iii) All participants participated in a fMRI session in which we measured brain responses to four runs of sweeping bar stimuli (referred to as the pRF mapping experiment). Eye tracking during scanning revealed no significant difference in fixation performance between groups: mean number of saccades in children was 1.48 ± 0.44, and in adults was 0.5 ± 0.28; $t(39) = 1.4$, *not significant.*

Following data quality thresholds discussed below, 8 children and 3 adults were excluded from further analysis in order to ensure similar pRF model fits in adults and children. Thus, subsequent analyses were done in 18 children and 23 adults. These numbers represent subjects who moved less than 2 voxels during retinotopic mapping and were able to fixate during mapping (fewer than 2 saccades); see Fig. S1.

2.2. Visual stimuli

For the pRF mapping experiment, the goal was to model in every voxel the region of the visual field that elicits a response from that voxel, namely its population receptive field (pRF). Subjects completed 4 runs of an experiment in which they fixated on a central stimulus and were required to indicate via a button-press when the central stimulus changed color. Black and white checkerboard bars (width $= 2^\circ$ of visual angle, length $= 14^\circ$) were swept across the screen during each run which lasted 3 min and 24 s. Bars swept the visual field in 8 different configurations in each run (4 orientations: 0°, 45°, 90°, 135°, each orientation was swept in 2 directions that were orthogonal to the bar). Same as (Dumoulin and Wandell, 2008; Gomez et al., 2018; Weiner and Grill-Spector, 2011).

2.3. Eye tracking

Eye tracking and fixation task performance were collected on a subset of children and adults. Fixation performance was tracked with the Eyelink software (http://www.sr-research.com/). Blinks, labeled by the Eyelink software, were removed from the timecourse data of the recorded eye by scrubbing with a 100 ms window on either end of the blink. Fixation data was then plotted for each subject. Only subjects that made fewer than three saccades (2° in size) during a mapping run were included for analysis. Due to the scanner environment, size of participants' head, and time constraints, not all subjects could be eye tracked during pRF mapping (eye tracking data was obtained for 25 children and 6 adults). Fixation task performance was collected on a subset (8 children, 7 adults) of subjects due to button box malfunction. All subjects, however, were trained on proper fixation technique outside the scanner using an eyetracker in the lab room.

2.4. Functional MRI parameters

Data were collected on a 3-Tesla GE Discovery MR750 scanner (GE Medical Systems) at the Center for Cognitive Neurobiological Imaging at Stanford University using a phase-array 16-channel surface coil. Functional data for the pRF mapping experiment were collected with 2.4 mm isotropic voxels (28 slices) in a slab oriented parallel to the parieto-occipital sulcus. Volumes were collected once every 2 s (2× acceleration factor). Subjects completed four runs of the pRF mapping experiment, each 3:24s in length.

2.5. Quantitative MRI

Quantitative MRI measurements were obtained from the protocols set forth in Mezer et al. (2013). T1 relaxation times were measured from four spoiled gradient echo (spoiled-GE) images with flip angles of 4, 10, 20, 30 (TR = 14 ms, TE = 2.4 ms) and a scan resolution of 0.8 mm × 0.8 mm x 1.0 mm. For the purposes of removing field inhomogeneities, we collected four additional spin echo inversion recovery (SEIR) scans with an echo planar imaging (EPI) read-out, a slab inversion pulse, and spectral spatial fat suppression. The SEIRs were acquired with a TR of 3.0 s, echo time set to minimum full, and 2× acceleration. The inversion times were 50, 400, 1200, and 2400 ms, and were collected at a 2.0 mm × 2.0 mm in-plane resolution and a slice thickness of 4.0 mm.

2.6. Anatomical MRI analysis

Both the spoiled-GE and the SEIR scans were processed using the mrQ software package in MATLAB to produce T1-weighted maps (Mezer et al., 2013). The mrQ analysis pipeline corrects for RF coil bias using SERI-EPI scans, producing accurate proton density (PD) and T1 fits across the brain. The full analysis pipeline and its published description can be found at (https://github.com/mezera/mrQ). An artificial T1-weighted anatomy was produced for each subject from these quantitative measures, which was used for cortical surface reconstruction and visualization of retinotopic data. Anatomical images for each subject were segmented through FreeSurfer (https://surfer.nmr.mgh.harvard.edu/), the resultant tissue segmentation was hand-corrected for classification errors. Functional data were restricted to the cortical ribbon by growing a 3-voxel thick (1 mm isotropic voxels) ribbon from the gray-white matter boundary.

2.7. Functional data processing and modeling

Data were processed and analyzed in MATLAB using mrVista software (http://github.com/vistalab) as in previous publications (Gomez et al., 2018; Natu et al., 2016). Functional data were aligned to the artificial T1-weighted volume. Functional data were unsmoothed, always analyzed within the individual's native brain space, and were restricted to the cortical ribbon.

Functional data were motion-corrected both within and between scans. Any subjects who moved more than 2 voxels within a scan were either excluded from data analysis or invited back for another session. In order to match for variance-explained in V1 and make sure that resultant development effects don't result in differences in pRF model fit, 8 children and 3 adults were excluded. Children and adults were thus matched for data quality as measured by no significant difference in variance-explained by the pRF model within V1 ($p = 0.11$), or across any ROI as assessed with an analysis of variance ANOVA. For the remaining subjects, there was no significant difference in motion during scanning between groups (adult motion average: 0.7 mm ± 0.33 mm, child: 0.89 mm ± 0.2 mm; $t(39) = 1.4$, n.s.), and no significant differences in explained variance across age-groups ($F(1,222) = 0.4$, *n.s.*) in an ANOVA run across all visual field maps. We report in Fig. 1 several summary properties of visual field maps in the lateral stream: volume of visual field maps, fraction retinotopically-driven (e.g., the number of above-threshold voxels normalized by total number of voxels within an ROI), and mean variance-explained by the pRF model within a map.

2.8. Estimating the population receptive field (pRF)

After functional data were transformed to the whole brain anatomy and restricted to the cortical ribbon, a pRF model was fit in each voxel (Dumoulin and Wandell, 2008). For each voxel, a 2-dimensional Gaussian receptive field is modeled, having a center described by x and y coordinates and σ describing the width, and a parameter, g, describing its gain. An additional variable is fit for each voxel describing a compressive summation exponent that describes nonlinear summation properties of cortical RFs in higher stages of the visual hierarchy (Kay et al., 2015, 2013). A candidate timecourse is produced from this pRF by convolving an HRF with the product of the stimulus movie and the pRF. The variables x, y, and σ are swept until the variance-explained of the voxel's timecourse is maximized by the pRF model, at which point the compressive term is likewise fit.

2.9. Voxel inclusion criteria

Voxels were only included for subsequent analyses if: (i) the variance-explained by the pRF model was greater than 5%, (ii) if their pRF center was within the stimulated visual field (≤7° radial eccentricity), and (iii) if their σ was greater than the model's floor value (0.21°).

The variance-explained threshold was chosen based on an approach that we utilized previously (Gomez et al., 2018). We evaluated the distribution of the variance-explained of non-retinotopic voxels in an ROI encompassing primary auditory cortex. To do so, we projected the FreeSurfer ROI in the superior temporal gyrus ROI that encompasses A1 from the FreeSurfer average cortical surface into each subject's native cortical surface. In each voxel of this ROI we evaluated the variance-explained of the pRF model. Across all subjects, the vast majority of voxels in this ROI had a variance-explained of zero, and the variance-explained in 94.4% of the voxels was less than 5%. This analysis demonstrates the sufficiency of this threshold to exclude non-retinotopic voxels. With this threshold, we also find a similar number of voxels in retinotopic areas of children and adults, which enables a fair comparison across age-groups.

2.10. pRF size versus eccentricity fits

To evaluate the relationship between a pRF's size and its eccentricity, all voxels that passed the inclusion criteria within an individual's ROI were entered into a linear regression in which each voxel's contribution was weighted by the variance-explained of the pRF model. The line-of-best fit was derived in each subject for each ROI, and then the slope and intercept of this line was averaged across participants of each age group.

2.11. Visual field coverage

To calculate the visual field coverage (VFC) for a given ROI and subject, we include all voxels in an ROI that passed the inclusion criteria. Voxels were modeled as a Gaussian with a peak normalized to 1. The VFC is produced at each point by averaging across pRFs' Gaussians that cover that point, and then normalizing by the maximum coverage value in that subject. We also implemented a bootstrapping procedure (Winawer and Witthoft, 2015) that draws with replacement n voxels from a subject's ROI of size n voxels, and produces an average VFC from 50 iterations to reduce the effect of outlier voxels. The average VFC from this bootstrapping approach is the VFC used for each subject's data.

To produce the average VFC of subjects in each age group, the VFC is averaged across hemispheres within a subject (by flipping the right hemisphere data along the vertical meridian and averaging with the left hemisphere) and then average across subjects of an age group. For quantification purposes (Fig. S6), we calculated the average pRF coverage along iso-eccentricity bins in each subject, thus quantifying pRF coverage as a function of eccentricity. We used 5 iso-eccentricity bins per degree of visual angle (a bin width of 0.2°) so that we do not sample the visual field more densely than it was modeled (pRF size minimum in mrVista is 0.2°). We then averaged across subjects within a group within a given iso-eccentricity bin to produce 1-dimensional distributions in group representing pRF coverage from the fovea to the periphery (Fig. S6). Kolmogorov-Smirnov (K-S) tests were run across these coverage-by-eccentricity distributions pooled across subjects to quantify the significance of differences between groups in the coverage (Fig. S6).

2.12. Definition of visual field maps across the lateral stream

Maps of pRF phase and eccentricity were projected onto an inflated cortical surface reconstruction for each subject. Borders between

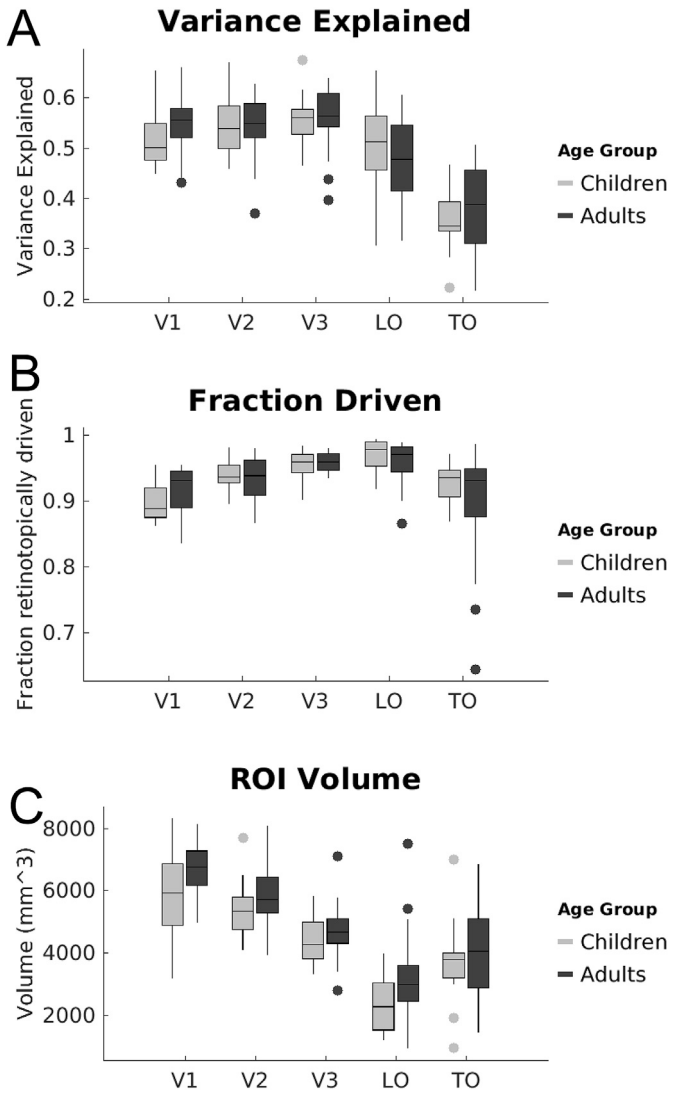

Fig. 1. Volume, fraction retinotopically driven, and the percent-variance-explained by the pRF model in the lateral visual stream. (A) Box plots of the proportion variance-explained. For each subject, we calculated the variance-explained by the pRF model in each voxel, then data were averaged across voxels in each visual field map/cluster within a participant, and then averaged across participants of each age group. The variance-explained significantly varied by region (main effect of ROI $F(4,222) = 49.2$, $p < 10–5$), but did not vary with age ($F(1,222) = 0.4$,$p = 0.53$), and there was no significant age by region interaction ($F(4,222) = 1.15$, $p = 0.33$). Number of subjects per ROI: V1-V3, Children = 18, Adults = 21; LO, Children = 16, Adults = 21; TO, Children = 14, Adults = 20. (B) For each visual field map, we calculated the fraction of voxels whose variance-explained by the pRF model was greater than 5% over the total number of voxels. Data are averaged separately across subjects in each age group. The fraction retinotopic voxels significantly varied by region (main effect of ROI: $F(4,222) = 16.4$,$p < 0.001$), but it did not vary across age groups (main effect of age, $F(1,222) = 0.7$, $p = 0.4$) and there was no significant age by region interaction ($F(4,222) = 2.18$, $p = 0.07$). (C) Box plots of the volume in cubic millimeters of field maps V1 through TO. Central line denotes median, circles are outliers. The metrics reflect the bilateral region combined across hemispheres. We found significant main effects of ROI ($F(4,222) = 56.5$, $p < 10-10$) and age ($F(1,222) = 11.5$,$p = 0.001$), where visual field maps in adults were larger than children, but there was no significant age by region interaction ($F(4,222) = 0.34$, $p = 0.85$). Moreover, Bonferroni-corrected post-hoc t-tests reveal no significant between age-group difference of size within any individual visual field map/cluster.

retinotopic maps were drawn on the cortical surface.

2.12.1. *Definition of V1-V3*

The boundary of early retinotopic areas V1-V3 was defined as the center of polar angle reversals occurring at the vertical or horizontal meridian (Sereno et al., 1995; Wandell and Winawer, 2015; Witthoft et al., 2014). We delineated visual field representations using polar angle reversals near the following anatomical landmarks: V1/V2 ventrally on the superior portion of the lingual gyrus and dorsally on the inferior portion of the cuneus, V2/V3 ventrally near the lingual sulcus and dorsally near the superior portion of the cuneus, V3/hV4 on the upper visual field representation on the lingual gyrus (Brewer et al., 2005).

2.12.2. *Definition of LO1/2*

LO1 was defined as a hemifield representation inferior to V3a; the lower field representation forms a boundary with the dorsal aspect of V3 (Larsson and Heeger, 2006; Sayres and Grill-Spector, 2008; Weiner and Grill-Spector, 2011). LO2 was defined as the subsequent hemifield, with the upper field representation forming the boundary between LO1 and LO2. In some cases, the upper field representation between LO1 and LO2 is not clear (see also (Hansen et al., 2007)) and this boundary was drawn at an oblique to horizontal phase. The eccentricity maps of the LO cluster is organized as follows: (i) the fovea is located posteriorly on the lateral surface, and is part of the confluent occipital fovea shared with V1, V2, and V3 and (ii) farther eccentricity bands are located more anteriorly and superiorly compared to the confluent fovea, ending on the middle occipital gyrus (Fig. 1B). The LO cluster was defined as the union of LO1 and LO2.

2.13. *Definition of TO1/2*

TO1 and TO2 are hemifield representations anterior to LO2, in and around the posterior aspect of the inferior temporal sulcus (ITS) (Amano et al., 2009). The boundary between TO1 and TO2 is the upper visual meridian which is typically located within the ITS. The posterior boundary of TO1 is the lower visual field representation which forms a boundary with LO2. The anterior boundary of TO2 is a separate lower field representation. The TO cluster was defined as the union of TO1 and TO2. It has a shared eccentricity map whereby the foveal representation is located inferiorly, close to or on the ITG from which eccentricity bands extend superiorly.

2.14. *Definition of the LO and TO clusters*

Because (i) the transition between LO1 to LO2 is sometimes difficult to observe, but because the transition between LO2 and TO1 is quite salient, and (ii) LO1 and LO2 share an eccentricity representation and TO1 and TO2 share a different eccentricity representation, we performed our analyses on the LO cluster, which is the combination of LO1 and LO2 and the TO cluster, which is the combination of TO1 and TO2. In this way, the LO map cluster extends from V3 dorsal to the crown of the middle occipital gyrus, and the TO cluster extends from the MOG into the periphery beyond the hMT + fovea (Fig. 2).

We also used an independent definition of the LO cluster from the Wang atlas definition of LO1 and LO2 (Wang et al., 2015), which overlaps our functionally-defined LO cluster to assess if using an ROI defined independently from the data had an impact on pRF quantification or developmental findings. Using cortex-based alignment in FreeSurfer (Fischl et al., 1999), we transformed the Wang LO1/2, itself produced from an average in an independent group of subjects, defined on the FreeSurfer average brain into each individual subject's brain and repeated analyses done for the functionally-defined LO. Results replicate those from the individually-defined LO cluster.

2.15. *Analysis of the relationship between the MOG and eccentricity maps*

To produce the observer-independent definition of the middle occipital gyrus used in the analyses, we used the FreeSurfer cortex-based alignment

algorithm. We defined the middle occipital gyrus on the FreeSurfer cortical average brain, then using cortex-based alignment, we transformed this anatomical label into each individual subject's native space. Resultant labels were transformed into binary NIFTI masks aligned to each subject's cortical surface on which the eccentricity of voxels derived from the pRF mapping experiment was plotted. Additionally, we compared the location of the MOG relative to the eccentricity maps in each subject.

2.16. Estimating spatial uncertainty using model-based decoding

To determine how changes in pRFs across development may impact information processing, we implemented a model-based decoding of spatial information as follows. We assessed mean spatial uncertainty of decoding a point target location across 1000 iterations for each subject and cluster. In each iteration, we evaluated how well the collection of the pRFs spanning each of the bilateral LO and TO clusters can resolve the location of a small target in the visual field. In each iteration, we randomly placed a small target (0.3° circle) in a 14° wide visual field. Then, we calculated the output of the response of each of the subject's pRFs in bilateral LO and TO clusters, respectively, to this stimulus. That is, for each pRF, we first calculated the product between the target and the pRF (pRF amplitude was normalized by its variance-explained) then added independent additive Gaussian noise, similar to (Kay et al., 2015). The noise had zero mean and a standard deviation of 20% of the maximum possible pRF value. To evaluate the population response of all pRFs within LO and TO clusters, respectively, the output response of each pRF is assigned to the center of the pRF in the visual field. This resulted in a response field representing how the collection of pRFs in a participant's cluster responds to the target. To predict the location of the target in the visual field from this response field, we calculated its center-of-mass (CoM). In other words, the CoM is our model's prediction of the target's location in the visual field. To evaluate the model's prediction error (spatial uncertainty), we calculated the distance between the predicted CoM to the actual target's position. We stored the spatial uncertainty for each iteration. We then calculated the mean spatial uncertainty for each subject's LO and TO clusters, respectively, for target positions in different eccentricity bins ranging from the fovea (0–2°) to the periphery (7°) in 1° steps. When matching for number of voxels across children and adults in LO, we repeated the analysis using a bootstrap approach (n = 1000) using a subset of voxels from the ROI (whose number was determined by the number of voxels from the subject with the smallest ROI, a child) without replacement on each iteration of the simulation.

2.17. Quantification and statistical analysis

2-way analyses of variance (ANOVAs) were run with grouping variables of visual field map (or cluster) and age-group. In order to maximize the number of subjects for each analysis (and minimize the variability in subject number across regions), data was averaged across hemispheres. 2-way ANOVAs were run for total visual field coverage (VFC) area with grouping variables of age-group and cluster. ANOVAs are robust against modest deviations from normality, and no data populations have any gross violation of normality (individual subjects or violin plots are illustrated in figures). All posthoc t-tests conducted were two-tailed. KS-tests for pRF coverage differences across age groups were run across distributions including data from each subject, rather than run on the group average, to better incorporate intersubject variability when comparing groups.

Bootstrapping methods were used to produce VFC plots to ensure robustness of fits and downweight outlier voxels; this bootstrapping method is described in the section on visual field coverage, above.

All errorbars in the main and figures represent standard error of the mean across subjects.

3. Results

We used fMRI to measure cortical responses in 26 children ages 5–12 years (mean age 8.5 ± 2.2 years, 12 females) and 26 adults ages 22–28 years old (mean age 24 ± 1.6 years, 9 females) while they fixated on a central stimulus and viewed a flickering checkerboard bar that swept the visual field. The timecourse of response in each voxel was modeled using a Gaussian pRF with a compressive spatial summation (Kay et al., 2013).

We first verified that MRI data quality was not lower in children than adults. Due to excessive motion (>2 voxels) during fMRI, data from 3 out of 26 adults and 8 out of 26 children were removed from further analysis. In the remaining 18 children (ages 5–12, mean ± std, 8.8 ± 2.1, 12

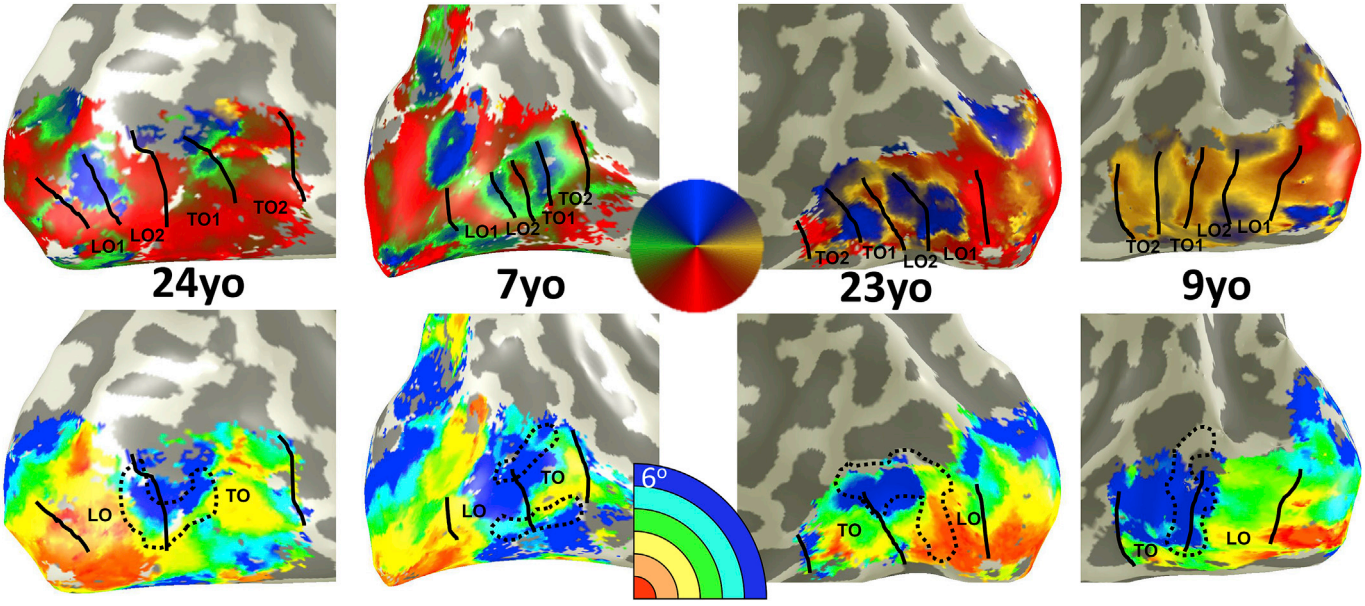

Fig. 2. Lateral eccentricity and polar angle maps are qualitatively similar across children and adults. From left to right, example phase (top) and eccentricity (bottom) maps showing the right hemisphere of an adult, right hemisphere of a child, left hemisphere of an adult, and left hemisphere of a child. Participant age depicted in black text. On phase maps (top row) LO1/2 and TO1/2 maps are drawn along phase transitions. Phase colormap illustrated in central circle. On eccentricity maps (bottom row), the transition from the LO maps cluster to the TO map cluster is drawn alongside a black dotted outline of the middle occipital gyrus in each subject. In every subject, the transition from LO to clusters occurs within the middle occipital gyrus.

female) and 23 adults (ages 22–27, 23.7 ± 1.4, 11 female) we found no significant differences in motion during scan ($t(39) = 1.4$, *n.s.*; Fig. S1B). Both children and adults maintained fixation during pRF mapping. There were no significant differences between age groups in eye movements during scan as we reported previously (Gomez et al., 2018); see Fig. S1. Additionally, there was no significant differences across age groups in the variance-explained by the pRF model (Fig. 1A) or the fraction of retinotopically driven voxels in either V1 alone or across all ROIs of the lateral visual stream (Fig. 1B). Thus, any developmental differences we observe are not a result of data-quality differences between age groups.

3.1. Does the topography of LO and TO visual field maps develop?

Previous studies reported stable visual field map topography in early visual cortex after age five (Conner et al., 2004; Gomez et al., 2018). However, it is unknown if intermediate and higher-level areas of the lateral visual stream develop during childhood. Thus, in each participant, we generated maps of pRF eccentricity, phase, and size (Fig. 2, Figs. S2–S4) and defined visual field maps of the lateral stream: V1, V2, V3, LO1/2, and TO1/2 (Fig. 2, Fig. S2). For quantification purposes, we consider two clusters: the lateral occipital cluster (LO combining LO1 and LO2) and temporal occipital cluster (TO combining TO1 and TO2). The number of above-threshold voxels in LO and TO did not significantly differ between children and adults ($F(1,74) = 2.7$, $p = 0.1$).

We first examined if there are developments in the spatial topography of these maps and in structural-functional correspondences. Data reveal three topographic features of LO and TO clusters that are stable across children and adults. First, in all participants there are separate foveal representations – one for the LO cluster in the occipital lobe, which is part of the confluent fovea, and another one for the TO cluster in the inferior temporal gyrus (Figs. 2, 3A, S3). Second, in all participants, from these inferiorly located foveal representations, more peripheral eccentricity bands emanate superiorly (Figs. 2, 3A, S3). Third, in all participants the transition between the LO and TO clusters is an eccentricity reversal, which is associated with a peripheral representation.

In the ventral stream, the transition between ventral occipital maps (hV4, associated with the confluent fovea) and temporal maps (VO1/2, associated with the VO fovea) shows a consistent structural-functional relationship (Witthoft et al., 2014). That is, the peripheral bands of hV4 and VO1 maps collide on the posterior transverse collateral sulcus (ptCoS). As the LO and TO map are also associated with separate foveal representations in different lobes, the occipital and temporal lobes, respectively, we sought to examine if such a structural-functional relationship also exists in the lateral stream.

Our data show that in both adults and children the representation of peripheral eccentricities of the LO and TO clusters consistently collide on a specific macroanatomical structure – the middle occipital gyrus (MOG; example subjects, Fig. 2; all subjects Fig. S3). To quantify functional and macroanatomical relationships in an observer-independent manner, we transformed the MOG defined anatomically in an independent cortical surface (FreeSurfer average brain, from 39 different adults (Fischl et al., 1999)) into each participant's cortical surface using cortex-based alignment, and then measured in each subject the distribution of pRF eccentricities within this independently-defined MOG. Our observations reveal three findings. First, in each participant and in both age groups, the MOG overlaps the peripheral eccentricity transition between the LO and TO eccentricity maps (Fig. 3A; all subjects Fig. S3). Second, in both children and adults, the distribution of pRF eccentricities in the MOG shows a peripheral bias (Fig. 3B): around 40% of voxels have an eccentricity that is larger than 5°. Due to limitations in the presentation setup in the MRI scanner, the periphery beyond 7° could not be measured, so any peripheral bias reported here is limited to this range. Third, examination of pRF eccentricities versus cortical curvature along a line ROI connecting the LO foveal representation to that of TO drawn in each subjects' brain, shows a consistent functional correspondence. That is, in a vast majority of subjects there is a negative correlation between curvature and eccentricity (Fig. 3C), with foveal representations residing in sulci (positive curvature) and more peripheral representations are on gyri (negative curvature). The distribution of these regression line slopes, fit in individual subjects, was significantly negative ($p < 0.00003$, *t*-test). Thus, the MOG is a reliable and developmentally-stable landmark for peripheral representations defining the transition between LO and TO clusters.

3.2. Do population receptive fields develop in the lateral visual stream?

We next sought to determine if there is quantitative development of pRFs across visual field maps spanning the lateral visual stream (V1 through TO). Thus, we measured in each participant mean pRF eccentricity, mean pRF size, and their relationship in each visual field map/cluster (V1 through TO), and compared values across children and adults.

Focusing first on pRF size across all visual field maps/clusters of the lateral stream (V1, V2, V3, LO, TO), we found a differential development of pRF size across the lateral stream (2-way ANOVA with factors of age-group and ROI, significant age-group by visual field map interaction:

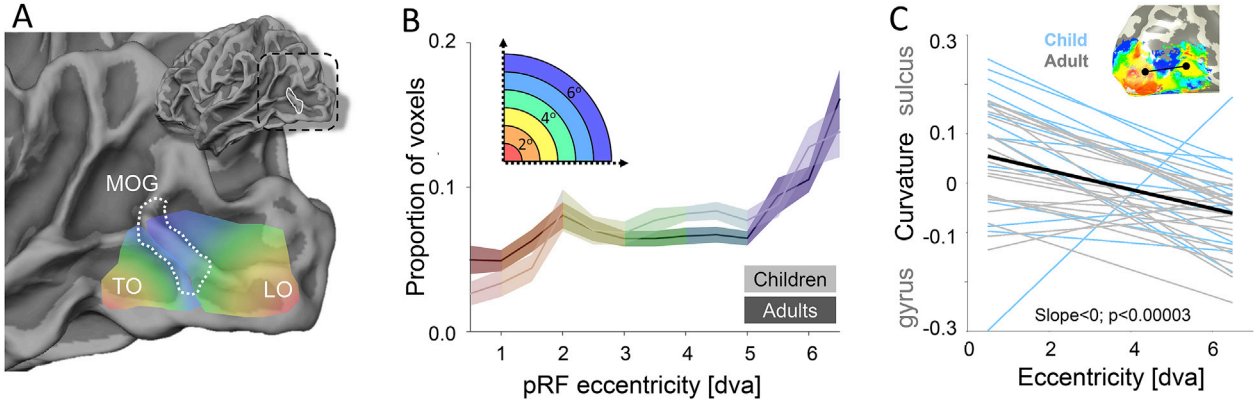

Fig. 3. Quantification of the relationship between cortical folding and visual field maps in lateral occipitotemporal cortex. (A) Illustration of the collision between the two eccentricity representations of the LO and TO clusters. The middle occipital gyrus (MOG) is outlined in a white dotted line, and marks the point where the LO periphery transitions into the TO representation of the peripheral visual field. (B) Average (solid line) and standard error (shaded regions) of histograms representing the eccentricity of pRF centers from voxels within the FreeSurfer defined MOG within children (lighter colors) and adults (darker colors). Histograms are colored according to eccentricity values. (C) The correlation between a voxel's eccentricity and its local curvature taken from voxels within a line ROI interconnecting the two foveal representations of LO and TO (inset: example line ROI in a single subject). Negative curvature values indicate gyri and positive values indicate sulci. Individual correlation lines for each subject are shown in gray for adults and blue for children, and the mean regression line (produced by averaging the slope and intercept values of individual line-of-best-fits) is shown in black. T-test indicates that the distribution of slope values from individual subjects is significantly negative.

$F(4,195) = 3.22$, $p < 0.05$). However, post-hoc t-tests reveal there were no significant differences in pRF size across age groups in earlier stages of the hierarchy (values for V1-V3 were reported previously (Gomez et al., 2018)). Thus, we ran a separate analysis focusing on the higher-level regions of the lateral stream. A 2-way ANOVA on pRF size in LO and TO clusters revealed a significant age group by ROI interaction ($F(1, 78) = 4.84$, $p = 0.03$), whereby pRFs in TO increased in size with age but pRFs in LO did not (Fig. 4A).

We also found a differential development of mean pRF eccentricity. Mean pRF eccentricity in V1 through TO1 showed an age by ROI interaction ($F(4,195) = 2.4$, $p = 0.05$), and no main effect of age ($F(1,195) = 0.84$, *n.s.*). Since there was no developmental change in V1-V3 as we previously reported (Gomez et al., 2018), these interactions are likely driven by developmental changes in the LO and TO clusters. Indeed, a 2-way ANOVA on mean eccentricity in LO and TO clusters revealed a significant age by ROI interaction ($F(1,78) = 3.91$, $p < 0.05$), with pRFs becoming more eccentric in TO with development, and less eccentric in LO (Fig. 4B).

Despite developmental differences in mean pRF properties in LO and TO clusters, the relationship between pRF size and eccentricity was developmentally stable. In both age groups pRF size linearly increases with pRF eccentricity. Within each of the LO and TO clusters, more peripheral pRFs were larger than those near the fovea (Fig. 4C–D, S3-S4). These linear relationships were remarkably consistent across age-groups with no significant difference between groups in either slopes or intercept of the linear fits (2-way ANOVA with factors of age and ROI: no significant main effect of age $F(1,216) = 0.11$, n.s.).

We also tested for correlations between pRF properties and age in LO/TO. In TO, there was no significant correlation between age and either mean pRF eccentricity (Pearson's $r = 0.18$, *n.s.*) or mean pRF size ($r = 0.3$, *n.s.*). Likewise, in LO, there was no significant correlation between age and either mean eccentricity ($r = -0.06$, *n.s.*) or mean size ($r = 0.01$, *n.s.*).

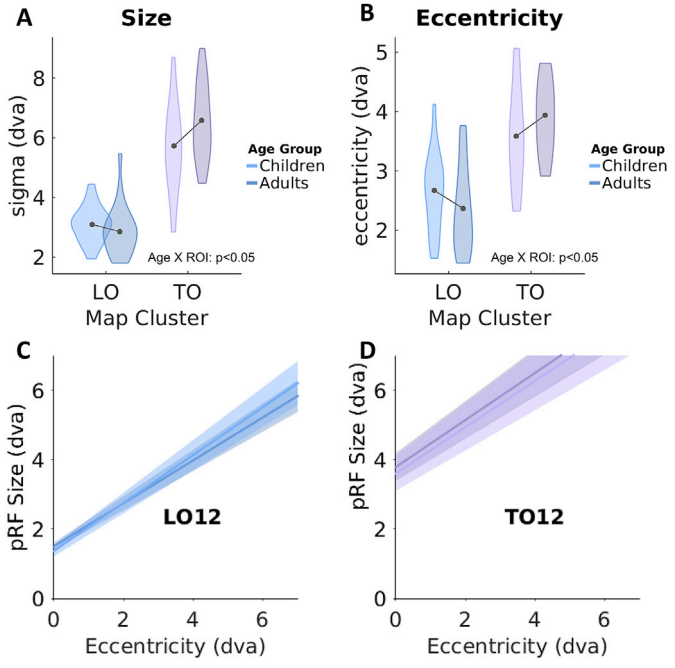

Fig. 4. pRF properties of the LO and TO clusters in children and adults. Quantification of mean pRF size (A) and mean pRF eccentricity (B) in the LO and TO clusters. Violin width denotes subject density. Lighter colors: children; Darker colors: adults. Dva: degrees of visual angle. (C–D) Average linear fits of pRF size vs. eccentricity. In all plots there are two lines: one for children (lighter) and one for adults (darker). Dark central lines: group average; shaded regions denote standard error across subjects. LO data include 16 children and 21 adults; TO data include 14 children and 20 adults.

To test the reliability of results, we analyzed the data using independent probabilistic maps of LO from the Wang retinotopic atlas derived from a different set of adult participants (Wang et al., 2015). This control analysis was done just for LO because the probabilistic maps of TO in the Wang atlas (Wang et al., 2015) do not contain enough overlap across subjects to produce reliable ROIs in individual subjects. Analysis of pRF properties in the independently-defined LO yielded the same results. Similar to our analysis above (Fig. 4C), in the ROIs defined from the Wang atlas there was no significant development in LO in the linear relationship between pRF size and eccentricity (intercept: $t = 0.6$, $p = 0.6$; slope $t = 0.87$, $p = 0.38$, Fig. S5A). Additionally, there was no significant difference in mean pRF size ($t(77) = 0.8$, $p = 0.4$, Fig. S5B) or mean pRF eccentricity ($t(77) = 1.7$, $p = 0.1$, Fig. S5C), across functionally- or independently-defined LO. These results demonstrate that pRF properties, and thus developmental findings, are not influenced by hand-drawn map borders.

3.3. How does pRF development affect visual field coverage in LO and TO?

As we found development of mean pRF size and eccentricity in LO and TO maps, we examined how this development may affect the tiling of the visual field, that is, the visual field coverage (VFC) obtained by the collection of pRFs spanning each of the LO and TO clusters. In both children and adults, the LO cluster had extensive coverage of the lower, contralateral, and central visual field (Fig. 5A-top). Likewise, in both age groups the TO cluster had a predominately contralateral hemifield representation, which had greater upper and peripheral VFC than LO (Fig. 5A-bottom). Nonetheless, the VFC coverage was more extensive in adults than children. To visualize from which portions of the visual field these differences arise, we plot for both LO and TO the difference in VFC between adults and children (Fig. 5B). In both LO and TO clusters, the VFC extended more into the ipsilateral visual field in adults than children. Developmental increases in the VFC in LO were near the central visual field, while those in TO were more peripheral (Fig. 5B), mirroring the interactions reported in Fig. 4. We quantified the development of VFC by calculating the average pRF coverage along iso-eccentricity rings within the visual field (Fig. S6). Results reveal significantly larger pRF coverage in adults than children in both LO (K-S test comparing the adult and child pRF coverage-by-eccentric curves $p < 0.005$) and TO ($p < 0.01$). In LO, pRF-coverage differences between children and adults are largest within the central 3° of the visual field, while differences in TO are largest around 3.5° and extend to the periphery (Fig. S6).

We performed a number of control analyses to ensure VFC differences are not driven by spurious between-group differences. Specifically, we tested whether differences in ROI size or measurement noise may explain between-group differences. First, examination of the relationship between ROI size (number of above-threshold voxels) and total VFC (area-under-the-curve derived from coverage of all pRFs in an ROI in each subject) revealed that participants with larger ROIs had larger total VFC (LO, $r = 0.7$, $p < 0.0001$; TO, $r = 0.44$, $p = 0.004$). To examine if this drives the developmental differences, we compared the number of above-threshold voxels in each cluster between age groups. Notably, there was no significant between-group difference in the number of above-threshold voxels in either LO ($t(39) = 1.38$, $p = 0.17$) or TO ($t(39) = 0.3$, $p = 0.78$). Therefore, developmental differences in total VFC cannot be explained by ROI size. Second, we examined if there is a correlation between total VFC and variance-explained by the pRF model. The analysis revealed no significant correlation in TO ($r = -0.04$, $p = 0.8$). While we found a general negative correlation between total VFC and variance-explained in LO ($r = -0.36$, $p = 0.02$) when including all subjects, this correlation cannot explained by developmental differences as there were no significant differences in variance-explained across age groups ($t(39) = 0.34$, $p = 0.74$). Furthermore, within children, there was no significant correlation between total VFC and age (LO, $r = -0.05$, $p = 0.86$; TO, $r = -0.2$; $p = 0.4$). Lastly, we compared the relationship between total VFC and average within-scan motion during

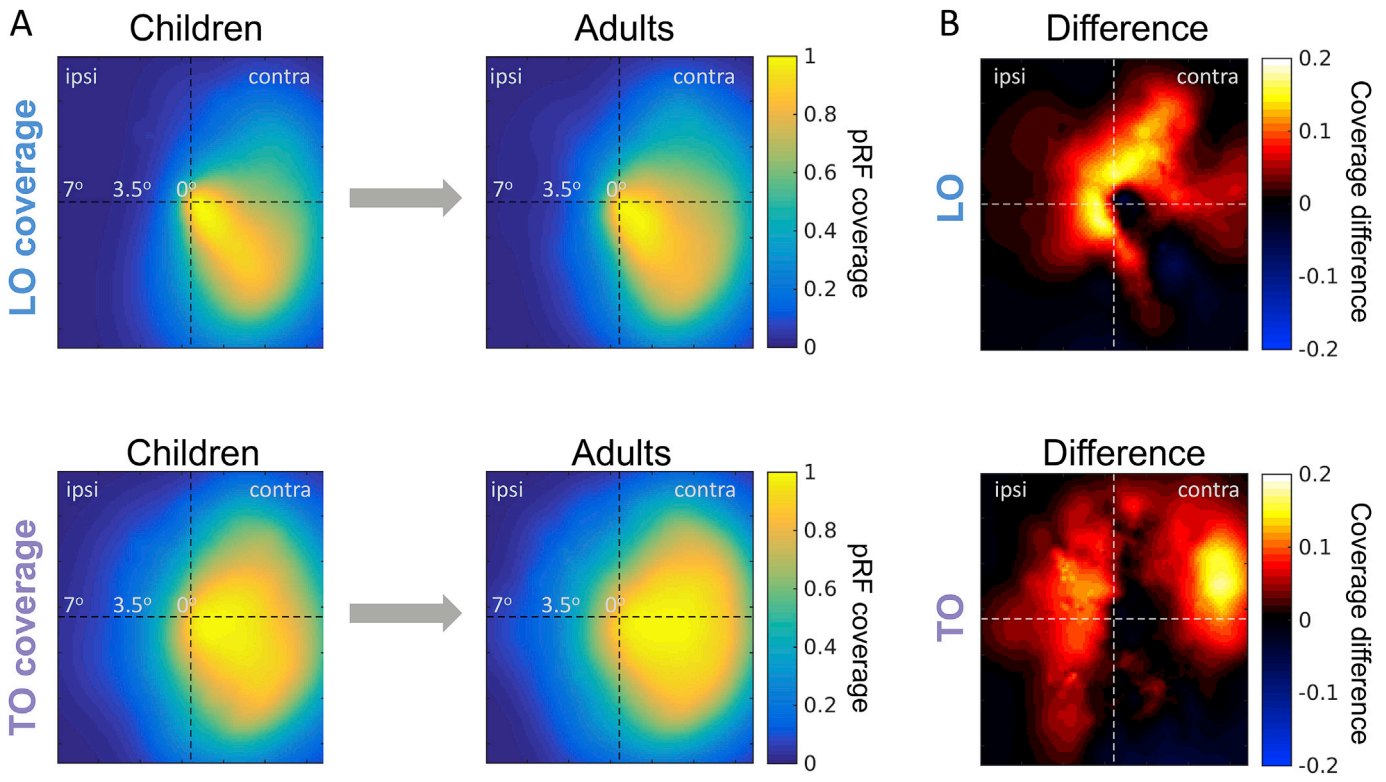

Fig. 5. Developmental increases in visual field coverage by pRFs in LO and TO clusters. (A) Visual field coverage in children (left) and adults (right) in the LO (top) and TO (bottom) clusters. For these plots, pRF coverage is averaged and normalized by the maximum in each subject and then averaged across age groups. Right hemisphere data is flipped and averaged with the left hemisphere. (B) Pointwise differences in LO and TO coverage between adults and children. Positive values indicate greater coverage in adults. LO data includes 16 children and 21 adults; TO data includes 14 children and 20 adults.

pRF mapping. For LO, there was no significant correlation ($r = 0.06$, $p = 0.73$). For TO, we observed a modest negative correlation ($r = -0.33$, $p = 0.03$), which was driven by two outliers (one child, one adult). Removing these two subjects revealed no significant correlation between total VFC and motion ($r = -0.15$, $p = 0.34$) and repeating the VFC comparison after removing these two participants still revealed a significant difference between groups (KS-test, p-value < 0.02).

3.4. How does pRF development affect the spatial precision of distributed responses?

Prior results suggest that the manner in which pRFs tile the visual field may affect decoding of spatial location from distributed activity across the voxels of a given brain region (Kay et al., 2015). Thus, we next asked if developmental increases in coverage affect spatial decoding from distributed LO and TO responses. To evaluate the spatial precision of decoding from distributed responses, we used a model-based decoding approach (Kay et al., 2015) to estimate how accurately the set of pRFs spanning LO or TO predict the location of a point target.

In brief, we evaluated how well the collection of pRFs spanning each of bilateral LO and TO clusters resolve the location of a small target in the visual field. In each iteration of the simulation, per subject, we randomly placed a small target (0.3° circle) within a region in the visual field spanning 14°. Then, we calculated the output of the response of each of the subject's pRFs in each of the LO and TO clusters based on the overlap between the target and the pRF plus additive Gaussian random noise. The predicted target's location is based on spatial summation of all pRF locations in a cluster weighed by their response magnitude, which we refer to as center of mass (CoM, Fig. 6A). For quantification, we calculated the spatial error between this predicted location and the actual location of the target, and averaged across 1000 iterations per subject and cluster (Fig. 6A).

Results reveal three important findings. First, spatial decoding error in both LO and TO increases with target eccentricity in both children and adults (Fig. 6B–C; 3-way ANOVA with factors of ROI, target eccentricity, age-group: main effect of eccentricity $F(4,394) = 253$, $p < 10^{-10}$). Second, despite the larger pRFs in TO compared in LO, spatial error is lower in TO compared to LO (compare Fig. 6B and C, main effect of ROI: $F(1,394) = 150.3$, $p < 10^{-10}$). For example, at 3.5° eccentricity, spatial decoding error in TO is half of LO. Third, spatial decoding error in predicting the target position from pRFs in LO and TO clusters is significantly higher in children than adults (main effect of age-group: $F(1,394) = 17.5$, $p < 0.0005$). Main effects of age-group remain significant in ANOVAs run independently in LO ($F(1,190) = 9.05$, $p = 0.003$) and TO ($F(1,190) = 7.25$, $p = 0.008$). That is, distributed responses in adult LO and TO better predict the spatial location of a point target on average by 0.5° in LO and 0.23° in TO. In contrast, spatial decoding error obtained by V1 pRFs does not change significantly with age ($F(1,195) = 2.96$, *n.s.,* data not shown), suggesting that this development is specific to high-level visual field maps that exhibit development in pRF properties and VFC.

To further test whether between-group differences in spatial decoding are of developmental origin rather than other factors, we examined if variance-explained by the pRF model, ROI size, or motion during scan could account for the decoding results. Analysis of the relationship between spatial decoding performance and average variance-explained by the pRF model across all participants found no correlation in TO ($r = 0.14$, $p = 0.38$) and a positive correlation in LO ($r = 0.33$, $p = 0.037$). However, in LO there were no significant differences in variance-explained across age groups. Further, children had higher spatial decoding error despite having numerically higher variance-explained compared to adults (Fig. 1). Analysis of the relationship between spatial decoding performance and ROI size (above threshold number of voxels) across all subjects revealed that decoding performance was generally better with more voxels (LO, $r = 0.58$, $p < 0.0001$; TO, $r = 0.31$, $p = 0.04$). However, again this is a general relationship that is not driven by group differences, as there was no significant between-group

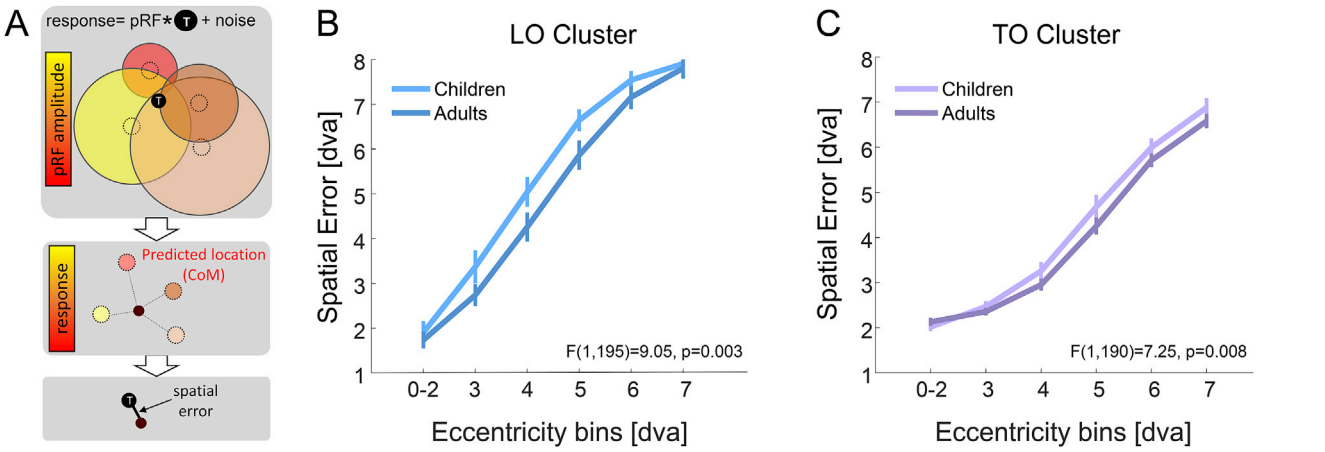

Fig. 6. Spatial error by pRFs spanning LO and TO map clusters decreases with age. (A) Schematic of the simulation to predict a target's location in the visual field relative to its actual location 'T'. Top: Colored circles represent pRFs, black circle represent target; response is estimated by convolving each pRF with the target and adding Gaussian random noise; responses are weighted by variance-explained; Middle: predicted location is the center of mass (CoM) of pRF responses across their locations. Bottom: spatial error is distance between predicted location and target location. (B) Spatial error in LO averaged in each binned ring of eccentricity across the visual field bilaterally in each subject in degrees of visual angle (dva) (C) Same as B, but for TO. Error bars represent standard error across subjects. Ns: LO, Children = 16, Adults = 21; TO, Children = 14, Adults = 20.

difference in the number of above threshold voxels. Nonetheless, to test this possibility explicitly, we performed a control analysis in which we compared decoding performance across groups using a constant number of voxels. The number of voxels was derived from the participant with the smallest ROI (see Methods). Even when matching ROI size, we again find better spatial decoding in adults than children ($F(1,195) = 7.8, p < 0.005$). Lastly, we found no significant correlations between average within-scan motion during pRF mapping and spatial decoding performance (LO, $r = -0.05$, $p = 0.77$; TO, $r = 0.25$, $p = 0.1$).

4. Discussion

Our data reveal four main findings. First, topographic organization of eccentricity and polar angle maps of the lateral stream are stable after age five. Second, by mapping visual field maps in the lateral stream for the first time in a large cohort of subjects across age groups, we observed a novel and developmentally stable structural-functional coupling: the MOG marks the transition between the peripheral representation of lateral occipital and temporal eccentricity maps. Third, we discovered that pRFs in LO and TO clusters — late stages of the lateral visual stream—undergo differential pRF development from childhood to adulthood, increasing coverage of the visual field centrally in LO and more peripherally in TO. Fourth, model-based decoding reveals that one consequence of this development is an improvement in the spatial precision of distributed visual representations in LO and TO clusters. Critically, these developments are likely not due to spurious between-group differences in motion, ROI size, or variance-explained by the pRF model.

4.1. Structural-functional coupling outside of primary sensory cortex

While primary sensory regions of human cortex are identifiable based on a specific cortical fold (e.g., primary visual cortex (V1) is in the calcarine sulcus, and primary somatosensory cortex (S1) is in the postcentral gyrus), classic theories suggest that structural-functional coupling is not prevalent across the brain (Glasser and Van Essen, 2011). However, recent results from our lab (Grill-Spector and Weiner, 2014; Rosenke et al., 2017; Witthoft et al., 2014) as well as others (Benson et al., 2014; Dumoulin et al., 2000; Frost and Goebel, 2013) have challenged this prevailing view. In the domain of visual field maps, we previously found that macroanatomical landmarks in the ventral stream predict transitions in eccentricity maps: the mid-fusiform sulcus (MFS) predicts the transition between foveal and peripheral representations (Weiner et al., 2014) and the posterior transverse collateral sulcus (ptCoS) predicts the eccentricity transition between ventral occipital and ventral temporal maps (Witthoft et al., 2014).

The discovery that the MOG marks the transition between lateral occipital and temporal maps mirrors the structural-functional coupling observed in the ventral stream and has three implications. First, it suggests that cortical folding predicts transitions in topographic maps and may be a prevalent organizational principle across the brain. This prediction can be tested in other systems. Second, since cortical folds form early in development (e.g., infants are born with all cortical folds (van der Knaap et al., 1996)), and eccentricity is coupled with cortical folding, it suggests that an eccentricity proto-map may be formed early in infancy and can guide other functional developments (Arcaro and Livingstone, 2017; Malach et al., 2002). Third, understanding structural-functional relationships may aid discerning the functional organization in the lateral stream, which has been debated (Amano et al., 2009; Brewer and Barton, 2012; Kolster et al., 2014), as well as identify regions in individual brains for which fMRI data acquisition is limited (e.g., patients).

4.2. Development in the lateral visual stream

To date, only a few studies have examined development of visual field representations in early visual cortex (Conner et al., 2004; Dekker et al., 2017; Gomez et al., 2018), only one study examined pRF development in the ventral stream (Gomez et al., 2018), and none have examined these developments in the lateral visual stream. While some aspects of our data show adult-like functional organization in children – for example, the organization of visual field maps in LO and TO clusters with respect to macroanatomy, other aspects of our data show development: pRF size, VFC, and spatial decoding in LO and TO clusters continue to develop after age 5. These findings suggest that the general topographic organization is laid out before age 5, but fine-scale properties, such as pRF distribution across the visual field and consequently, spatial decoding, continue to be fine-tuned after age 5. Future longitudinal studies examining pRF development within the same subjects will clarify when these pRF developments emerge, as our children included a relatively large age range from 5 to 12 years old.

Observing that pRFs undergo development in the lateral visual stream has two important implications. First, it provides evidence for a novel aspect of development in visual cortex that was previously undocumented. That is, not all visual streams implement the same pattern of pRF development. While pRFs in visual field maps in the ventral stream (hV4,

VO1) were developed by the age of five (Gomez et al., 2018), pRFs in the lateral stream show a more protracted development. Moreover, the LO and TO clusters implement different forms of pRF development, leading to greater coverage of the center in LO, but more peripheral regions of the visual field in TO in adults than children.

Second, finding pRF development in LO and TO challenges the notion that the lateral visual stream, containing brain regions involved in processing shapes (Grill-Spector et al., 1998a; Kourtzi and Kanwisher, 2001; Malach et al., 1995; Mendola et al., 1999) and motion (Huk et al., 2002; Tootell et al., 1995b), is developmentally stable after age 5. For example, motion-selective hMT+, which overlaps with the TO cluster, and object-selective LO, which overlaps with LO2 (Larsson and Heeger, 2006; Sayres and Grill-Spector, 2008), have been thought to develop early. Specifically, hMT+ is thought to be early-developed like V1, as it is myelinated at birth (Bartels and Zeki, 2005; Watson et al., 1993). Likewise, object-selectivity in LO is developmentally stable after age 7 (Golarai et al., 2007; Nishimura et al., 2015; Scherf et al., 2007). Future research examining other fine-scale properties such as sensitivity to shape in LO (Natu et al., 2016) or motion and speed direction in TO (Kamitani and Tong, 2006) can determine if additional fine-scale neural properties develop in the lateral visual stream. As pRFs play an important role in spatial integration, LO responses are correlated with object recognition (Grill-Spector et al., 2000), and hMT + responses are correlated with reading ability (Demb et al., 1998, 1997; Lovegrove et al., 1980; Rauschecker et al., 2011), our findings make a novel prediction: maldevelopment of pRFs in the lateral stream may lead to impoverished spatial integration and consequently object recognition and reading deficiencies. This hypothesis can be tested in future research.

4.3. A model relating pRF development to spatial encoding in the brain

As the first observation of pRF development in the lateral visual stream, these findings establish a novel bridge between childhood changes in pRFs to the development of spatial information. In both LO and TO clusters, there is a change in the distribution of pRFs across the visual field, however, unique development in each cluster results in a coverage change that emphasizes a different portion of the visual field. In TO, developmental increases in pRF size and eccentricity lead to increased coverage of the periphery. In the LO cluster, changes in the distribution of pRFs lead to improved coverage near the central visual field, especially the upper visual field.

We acknowledge that a limitation of our method is that we cannot infer from fMRI measurements of pRFs the development of individual neurons' RFs, as all the neurons in a voxel contribute to the population response, and thus the pRF is a measurement of the central tendency (Haak et al., 2012). Developmental changes we observe in pRFs of the lateral stream may thus result from a number of neuronal sources, such as changes in the scatter of RFs within a voxel or changes in neural RF size. We cannot disambiguate these possibilities with present measurements, as it is impossible to measure individual RFs non-invasively in humans. Furthermore, animal models, like the macaque, which enable measurements of single neuron RFs, do not possess the LO visual field maps. Thus, future methodological advancements will be necessary to determine what developmental changes in individual RFs contribute to the observed pRF development.

Nonetheless, our data show that pRF development affects the decoding of spatial location from distributed responses of pRFs spanning a visual field map cluster. That is, in both LO and TO clusters, developmental changes in the tiling of the visual field by pRFs result in improved spatial decoding of the location of items in the visual field. This observation has important implications for theories of position and size tolerance. While prevailing theories (Serre et al., 2007) suggest that systematic increases in pRF size across processing stages of visual hierarchies (Dumoulin and Wandell, 2008; Wandell and Winawer, 2015) reduce spatial precision by increasing position and size tolerance, we show that the common intuition that larger pRFs decrease spatial precision may be misleading. In fact, spatial precision is higher in TO than LO, despite the larger pRFs in the former than the latter. In other words, there is a distinction between the local scale (i.e., information carried by a single pRF) and the distributed scale (i.e., information carried by distributed responses across voxels spanning a map). At the local scale, individual pRFs in TO would show reduced sensitivity to stimulus location and size compared to LO due to increased pRF size. However, at the cluster scale, sensitivity to stimulus location in enhanced in TO due to increased pRF coverage and scatter in the periphery, which together provide a better tiling of the visual field. This leads to the following intriguing insight: spatial precision of distributed responses by a set of pRFs is determined not only by their size, but also by their scatter. In fact larger pRFs that are more scattered may produce better spatial precision than small spatially concentrated pRFs (Kay et al., 2015; Snippe and Koenderink, 1992).

Together, our findings establish an important basis for understanding development of the human visual system from childhood to adulthood, show the impact of cortical development on spatial coding, and provide an essential foundation for understanding developmental deficits.

5. Author contributions

JG designed the experiments, collected and analyzed the data, and wrote the manuscript. AD analyzed the data. BJ and MB collected the data. VN collected and analyzed the data. KGS designed the experiments, analyzed the data, and wrote the manuscript.

Acknowledgements

This research was funded by the NSF Graduate Research Development Program (grant DGE-114747) and Ruth L. Kirschstein National Research Service Award (grant F31EY027201) to JG, and the NIH (grants 1ROI1EY02231801A1, 1RO1EY02391501A1) to KGS and training grant 5T32EY020485 supporting VN.

Appendix A. Supplementary data

Supplementary data to this article can be found online at https://doi.org/10.1016/j.neuroimage.2018.11.056.

References

Amano, K., Wandell, B.A., Dumoulin, S.O., 2009. Visual field maps, population receptive field sizes, and visual field coverage in the human MT+ complex. J. Neurophysiol. 102, 2704–2718.

Arcaro, M., Livingstone, M., 2017. A hierarchical, retinotopic proto-organization of the primate visual system at birth. Elife 6. https://doi.org/https://doi.org/10.7554/eLife.26196.001.

Bartels, A., Zeki, S., 2005. The chronoarchitecture of the cerebral cortex. Philos. Trans. R. Soc. Lond. B Biol. Sci. 360, 733–750. https://doi.org/10.1098/rstb.2005.1627.

Battelli, L., Pascual-Leone, A., Cavanagh, P., 2007. The "when" pathway of the right parietal lobe. Trends Cognit. Sci. 11, 204–210.

Ben-Shachar, M., Dougherty, R.F., Deutsch, G.K., Wandell, B.A., 2011. The development of cortical sensitivity to visual word forms. J. Cognit. Neurosci. 23, 2387–2399.

Benson, N.C., Butt, O.H., Brainard, D.H., Aguirre, G.K., 2014. Correction of distortion in flattened representations of the cortical surface allows prediction of V1-V3 functional organization from anatomy. PLoS Comput. Biol. 10, e1003538. https://doi.org/10.1371/journal.pcbi.1003538.

Brewer, A., Barton, B., 2012. Visual field map organization in human visual cortex. In: Visual Cortex - Current Status and Perspectives. InTech. https://doi.org/10.5772/51914.

Brewer, A.A., Liu, J., Wade, A.R., Wandell, B.A., 2005. Visual field maps and stimulus selectivity in human ventral occipital cortex. Nat. Neurosci. 8, 1102–1109.

Cantlon, J.F., Pinel, P., Dehaene, S., Pelphrey, K.A., 2011. Cortical representations of symbols, objects, and faces are pruned back during early childhood. Cerebr. Cortex 21, 191–199. https://doi.org/10.1093/cercor/bhq078.

Conner, I.P., Sharma, S., Lemieux, S.K., Mendola, J.D., 2004. Retinotopic organization in children measured with fMRI. J. Vis. 4, 509–523. https://doi.org/10.1167/4.6.10.

Dekker, T.M., Schwarzkopf, D.S., Haas, B. de, Nardini, M., Sereno, M.I., 2017. Population Receptive Field Tuning Properties of Visual Cortex during Childhood bioRxiv 213108. https://doi.org/10.1101/213108.

Demb, J.B., Boynton, G.M., Heeger, D.J., 1998. Functional magnetic resonance imaging of early visual pathways in dyslexia. J. Neurosci. 18, 6939–6951.

Demb, J.B., Boynton, G.M., Heeger, D.J., 1997. Brain activity in visual cortex predicts individual differences in reading performance. Proc. Natl. Acad. Sci. U. S. A 94, 13363–13366.
Dumoulin, S.O., Bittar, R.G., Kabani, N.J., Baker Jr., C.L., Le Goualher, G., Bruce Pike, G., Evans, A.C., 2000. A new anatomical landmark for reliable identification of human area V5/MT: a quantitative analysis of sulcal patterning. Cerebr. Cortex 10, 454–463.
Dumoulin, S.O., Wandell, B.A., 2008. Population receptive field estimates in human visual cortex. Neuroimage 39, 647–660.
Fischl, Sereno, M.I., Dale, A.M., 1999. Cortical surface-based analysis. II: inflation, flattening, and a surface-based coordinate system. Neuroimage 9, 195–207. https://doi.org/10.1006/nimg.1998.0396.
Frost, M.A., Goebel, R., 2013. Functionally informed cortex based alignment: an integrated approach for whole-cortex macro-anatomical and ROI-based functional alignment. Neuroimage. https://doi.org/10.1016/j.neuroimage.2013.07.056.
Glasser, M.F., Van Essen, D.C., 2011. Mapping human cortical areas in vivo based on myelin content as revealed by T1- and T2-weighted MRI. J. Neurosci. 31, 11597–11616. https://doi.org/10.1523/JNEUROSCI.2180-11.2011.
Golarai, G., Ghahremani, D.G., Whitfield-Gabrieli, S., Reiss, A., Eberhardt, J.L., Gabrieli, J.D., Grill-Spector, K., 2007. Differential development of high-level visual cortex correlates with category-specific recognition memory. Nat. Neurosci. 10, 512–522.
Golarai, G., Liberman, A., Yoon, J.M., Grill-Spector, K., 2010. Differential development of the ventral visual cortex extends through adolescence. Front. Hum. Neurosci. 3, 80. https://doi.org/10.3389/neuro.09.080.2009.
Gomez, J., Natu, V., Jeska, B., Barnett, M., Grill-Spector, K., 2018. Development differentially sculpts receptive fields across early and high-level human visual cortex. Nat. Commun. 9. https://doi.org/10.1038/s41467-018-03166-3.
Goodale, M.A., Milner, A.D., Jakobson, L.S., Carey, D.P., 1991. A neurological dissociation between perceiving objects and grasping them. Nature 349, 154–156.
Grill-Spector, K., Golarai, G., Gabrieli, J., 2008. Developmental neuroimaging of the human ventral visual cortex. Trends Cognit. Sci. 12, 152–162.
Grill-Spector, K., Kourtzi, Z., Kanwisher, N., 2001. The lateral occipital complex and its role in object recognition. Vis. Res. 41, 1409–1422.
Grill-Spector, K., Kushnir, T., Edelman, S., Itzchak, Y., Malach, R., 1998a. Cue-invariant activation in object-related areas of the human occipital lobe. Neuron 21, 191–202.
Grill-Spector, K., Kushnir, T., Hendler, T., Edelman, S., Itzchak, Y., Malach, R., 1998b. A sequence of object-processing stages revealed by fMRI in the human occipital lobe. Hum. Brain Mapp. 6, 316–328.
Grill-Spector, K., Kushnir, T., Hendler, T., Malach, R., 2000. The dynamics of object-selective activation correlate with recognition performance in humans. Nat. Neurosci. 3, 837–843.
Grill-Spector, K., Weiner, K.S., 2014. The functional architecture of the ventral temporal cortex and its role in categorization. Nat. Rev. Neurosci. 15, 536–548. https://doi.org/10.1038/nrn3747.
Haak, K.V., Cornelissen, F.W., Morland, A.B., 2012. Population receptive field dynamics in human visual cortex. PLoS One 7, e37686. https://doi.org/10.1371/journal.pone.0037686.
Hansen, K. a, Kay, K.N., Gallant, J.L., 2007. Topographic organization in and near human visual area V4. J. Neurosci. 27, 11896–11911. https://doi.org/10.1523/JNEUROSCI.2991-07.2007.
Huk, A.C., Dougherty, R.F., Heeger, D.J., 2002. Retinotopy and functional subdivision of human areas MT and MST. J. Neurosci. https://doi.org/20026661.
Kamitani, Y., Tong, F., 2006. Decoding seen and attended motion directions from activity in the human visual cortex. Curr. Biol. 16, 1096–1102. https://doi.org/10.1016/j.cub.2006.04.003.
Kay, K.N., Weiner, K.S., Grill-Spector, K., 2015. Attention reduces spatial uncertainty in human ventral temporal cortex. Curr. Biol. 25, 595–600. https://doi.org/10.1016/j.cub.2014.12.050.
Kay, K.N., Winawer, J., Mezer, A., Wandell, B.A., 2013. Compressive spatial summation in human visual cortex. J. Neurophysiol. 110, 481–494. https://doi.org/10.1152/jn.00105.2013.
Kolster, H., Janssens, T., Orban, G.A., Vanduffel, W., 2014. The retinotopic organization of macaque occipitotemporal cortex anterior to V4 and caudoventral to the middle temporal (MT) cluster. J. Neurosci. 34, 10168–10191. https://doi.org/10.1523/JNEUROSCI.3288-13.2014.
Kourtzi, Z., Kanwisher, N., 2001. Representation of perceived object shape by the human lateral occipital complex. Science (80-.) 293, 1506–1509.
Kourtzi, Z., Kanwisher, N., 2000. Cortical regions involved in perceiving object shape. J. Neurosci. 20, 3310–3318.
Larsson, J., Heeger, D.J., 2006. Two retinotopic visual areas in human lateral occipital cortex. J. Neurosci. https://doi.org/10.1523/JNEUROSCI.1657-06.2006.
Lovegrove, W.J., Bowling, a, Badcock, D., Blackwood, M., 1980. Specific reading disability: differences in contrast sensitivity as a function of spatial frequency. Science 210, 439–440. https://doi.org/10.1126/science.7433985.
Malach, R., Levy, I., Hasson, U., 2002. The topography of high-order human object areas. Trends Cognit. Sci. 6, 176–184.
Malach, R., Reppas, J.B., Benson, R.R., Kwong, K.K., Jiang, H., Kennedy, W.A., Ledden, P.J., Brady, T.J., Rosen, B.R., Tootell, R.B., 1995. Object-related activity revealed by functional magnetic resonance imaging in human occipital cortex. Proc. Natl. Acad. Sci. U. S. A. 92, 8135–8139.
Mendola, J.D., Dale, A.M., Fischl, B., Liu, A.K., Tootell, R.B.H., 1999. The representation of illusory and real contours in human cortical visual areas revealed by functional magnetic resonance imaging. J. Neurosci. 19, 8560–8572. https://doi.org/10.1523/JNEUROSCI.19-19-08560.1999.
Mezer, A., Yeatman, J.D., Stikov, N., Kay, K.N., Cho, N.J., Dougherty, R.F., Perry, M.L., Parvizi, J., Hua le, H., Butts-Pauly, K., Wandell, B.A., 2013. Quantifying the local tissue volume and composition in individual brains with magnetic resonance imaging. Nat. Med. 19, 1667–1672. https://doi.org/10.1038/nm.3390.
Natu, V.S., Barnett, M.A., Hartley, J., Gomez, J., Stigliani, A., Grill-Spector, K., 2016. Development of neural sensitivity to face identity correlates with perceptual discriminability. J. Neurosci. 36, 10893–10907. https://doi.org/10.1523/JNEUROSCI.1886-16.2016.
Nishimura, M., Scherf, K.S., Zachariou, V., Tarr, M.J., Behrmann, M., 2015. Size precedes view: developmental emergence of invariant object representations in lateral occipital complex. J. Cognit. Neurosci. 27, 474–491. https://doi.org/10.1162/jocn_a_00720.
Peelen, M.V., Glaser, B., Vuilleumier, P., Eliez, S., 2009. Differential development of selectivity for faces and bodies in the fusiform gyrus. Dev. Sci. 12. https://doi.org/10.1111/j.1467-7687.2009.00916.x.
Raiguel, S., Van Hulle, M.M., Xiao, D.-K., Marcar, V.L., Orban, G.A., 1995. Shape and spatial distribution of receptive fields and antagonistic motion surrounds in the middle temporal area (V5) of the macaque. Eur. J. Neurosci. https://doi.org/10.1111/j.1460-9568.1995.tb00629.x.
Rauschecker, A.M., Bowen, R.F., Perry, L.M., Kevan, A.M., Dougherty, R.F., Wandell, B.A., 2011. Visual feature-tolerance in the reading network. Neuron 71, 941–953. https://doi.org/10.1016/j.neuron.2011.06.036.
Rosenke, M., Weiner, K.S., Barnett, M.A., Zilles, K., Amunts, K., Goebel, R., Grill-Spector, K., 2017. A cross-validated cytoarchitectonic atlas of the human ventral visual stream. Neuroimage. https://doi.org/10.1016/j.neuroimage.2017.02.040.
Sayres, R., Grill-Spector, K., 2008. Relating retinotopic and object-selective responses in human lateral occipital cortex. J. Neurophysiol. 100, 249–267.
Scherf, K.S., Behrmann, M., Humphreys, K., Luna, B., 2007. Visual category-selectivity for faces, places and objects emerges along different developmental trajectories. Dev. Sci. 10, F15–F30.
Sereno, M.I., Dale, A.M., Reppas, J.B., Kwong, K.K., Belliveau, J.W., Brady, T.J., Rosen, B.R., Tootell, R.B., 1995. Borders of multiple visual areas in humans revealed by functional magnetic resonance imaging. Science (80-.) 268, 889–893.
Serre, T., Oliva, A., Poggio, T., 2007. A feedforward architecture accounts for rapid categorization. Proc. Natl. Acad. Sci. U. S. A 104, 6424–6429. https://doi.org/10.1073/pnas.0700622104.
Snippe, H.P., Koenderink, J.J., 1992. Discrimination thresholds for channel-coded systems. Biol. Cybern. https://doi.org/10.1007/BF00204120.
Strappini, F., Pelli, D.G., Di Pace, E., Martelli, M., 2017. Agnosic vision is like peripheral vision, which is limited by crowding. Cortex. https://doi.org/10.1016/j.cortex.2017.01.012.
Tootell, R.B., Reppas, J.B., Dale, A.M., Look, R.B., Sereno, M.I., Malach, R., Brady, T.J., Rosen, B.R., 1995a. Visual motion aftereffect in human cortical area MT revealed by functional magnetic resonance imaging. Nature 375, 139–141. https://doi.org/10.1038/375139a0.
Tootell, R.B., Reppas, J.B., Kwong, K.K., Malach, R., Born, R.T., Brady, T.J., Rosen, B.R., Belliveau, J.W., 1995b. Functional analysis of human MT and related visual cortical areas using magnetic resonance imaging. J. Neurosci. 15, 3215–3230.
Ungerleider, L.G., Mishkin, M., 1982. Two cortical visual systems. In: Ingle, D.J., Goodale, M.A., Mansfield, R.J.W. (Eds.), Analysis of Visual Behavior. MIT Press, Cambridge, Massachusetts, pp. 549–586.
van der Knaap, M.S., van Wezel-Meijler, G., Barth, P.G., Barkhof, F., Adèr, H.J., Valk, J., 1996. Normal gyration and sulcation in preterm and term neonates: appearance on MR images. Radiology 200, 389–396. https://doi.org/10.1148/radiology.200.2.8685331.
Vinberg, J., Grill-Spector, K., 2008. Representation of shapes, edges, and surfaces across multiple cues in the human visual cortex. J. Neurophysiol. 99, 1380–1393.
Wandell, B.A., Winawer, J., 2015. Computational neuroimaging and population receptive fields. Trends Cognit. Sci. 19, 349–357. https://doi.org/10.1016/j.tics.2015.03.009.
Wandell, B.A., Winawer, J., 2011. Imaging retinotopic maps in the human brain. Vis. Res. 51, 718–737.
Wang, L., Mruczek, R.E.B., Arcaro, M.J., Kastner, S., 2015. Probabilistic maps of visual topography in human cortex. Cerebr. Cortex 25, 3911–3931. https://doi.org/10.1093/cercor/bhu277.
Watson, J.D., Myers, R., Frackowiak, R.S., Hajnal, J.V., Woods, R.P., Mazziotta, J.C., Shipp, S., Zeki, S., 1993. Area V5 of the human brain: evidence from a combined study using positron emission tomography and magnetic resonance imaging. Cerebr. Cortex 3, 79–94.
Weiner, K.S., Golarai, G., Caspers, J., Chuapoco, M.R., Mohlberg, H., Zilles, K., Amunts, K., Grill-Spector, K., 2014. The mid-fusiform sulcus: a landmark identifying both cytoarchitectonic and functional divisions of human ventral temporal cortex. Neuroimage 84, 453–465. https://doi.org/10.1016/j.neuroimage.2013.08.068.
Weiner, K.S., Grill-Spector, K., 2013. Neural representations of faces and limbs neighbor in human high-level visual cortex: evidence for a new organization principle. Psychol. Res. 77, 74–97. https://doi.org/10.1007/s00426-011-0392-x.
Weiner, K.S., Grill-Spector, K., 2011. Not one extrastriate body area: using anatomical landmarks, hMT+, and visual field maps to parcellate limb-selective activations in human lateral occipitotemporal cortex. Neuroimage 56, 2183–2199.
Winawer, J., Witthoft, N., 2015. Human V4 and ventral occipital retinotopic maps. Vis. Neurosci. 32, E020. https://doi.org/10.1017/S0952523815000176.
Witthoft, N., Nguyen, M.L., Golarai, G., LaRocque, K.F., Liberman, A., Smith, M.E., Grill-Spector, K., 2014. Where is human V4? Predicting the location of hV4 and VO1 from cortical folding. Cerebr. Cortex 24, 2401–2408. https://doi.org/10.1093/cercor/bht092.
Yeatman, J.D., Wandell, B.A., Mezer, A.A., 2014. Lifespan maturation and degeneration of human brain white matter. Nat. Commun. 5, 4932. https://doi.org/10.1038/ncomms5932.